**Proceedings of the ASME 2009 International Design Engineering Technical Conferences &
Computers and Information in Engineering Conference
IDETC/CIE 2009
August 30 - September 2, 2009, San Diego, California, USA**

DETC2009-86529

IMPEDANCE CONTROL OF MANIPULATORS WITH HEAVY PAYLOAD FOR SPACECRAFT RENDEZVOUS & DOCKING SIMULATORS

Farhad Aghili
Canadian Space Agency
Department of Space Technology
Saint-Hubert, Quebec, Canada J3Y 8Y9
Email: farhad.aghili@space.gc.ca

ABSTRACT

This paper presents a method to control a manipulator system grasping a rigid-body payload so that the motion of the combined system in consequence of external applied forces to be the same as another free-floating rigid-body (with different inertial properties). This allows zero-g emulation of a scaled spacecraft prototype under the test in a 1-g laboratory environment. The controller consisting of motion feedback and force/moment feedback adjusts the motion of the test spacecraft so as to match that of the flight spacecraft. The stability of the overall system is analytically investigated, and the results show that the system remains stable provided that the inertial properties of two spacecraft are different and that an upperbound on the norm of the inertia ratio of the payload to manipulator is respected. Important practical issues such as calibration and sensitivity analysis to sensor noise and quantization are also presented. Finally, experimental results are presented.

1 Introduction and Motivation

There are many technologies to address the problem of reproducing the micro-gravity space environment, such as air bearings, underwater test tanks, free-fall tests, and magnetic suspension systems. However, of these, only air bearings have proven useful for testing spacecraft. Achieving weightlessnees by using natural buoyancy facilities, i.e., water tank, has been used extensively for astronaut training. However, a functional spacecraft can not be submerged in the water, and in addition viscous damping does not allow a perfect force-free environment. A free-fall test through flying parabolas in aircraft can achieve zero-g in a 3-D environment. But only for brief periods. Magnetic suspension systems provide only a low force-torque dynamic environment with a small range of motion. Air-bearing tables (also known as planar air-bearings) [1, 2] and spherical air-bearings [3] are commonly used for ground-based testbeds for testing the translation and attitude control systems of a spacecraft. An emulation of zero-g translational motion can be achieved by an air-bearing table on which a spacecraft translates on a surface perpendicular to the gravity vector while being floated on a cushion of compressed air with almost no resistance. This technique has been used for testing various space systems such as formation flying [4], free-flying space robots [5], orbital rendezvous and docking [6], capturing mechanisms of spacecraft [7], and free-flying inspection vehicles [4]. Although the air-bearing table system can be utilized to test some physical components of spacecraft control systems including the sensors and actuators, this system is limited to a two-dimensional planar environment. Spherical air-bearings have been used for spacecraft attitude determination and control hardware/software verification for many years [3]. A spherical air-bearing yields minimum friction and hence offers a nearly torque-free environment if the center of mass is coincident with the bearing's center of rotation. The main problem with the air bearing system is the limited range of motion resulting from equipment being affixed to the bearing [8]. Also, spherical air-bearings are not useful for simulating spacecraft having flexible appendages, because the location of the center-of-mass of such spacecraft is not fixed. Although one can envisage combining the two air-bearing technologies in a testbed for reproducing

both the rotational and translational motions, complete freedom in all six rigid degrees-of-freedom is still technically difficult to achieve [3].

Motion table testing systems allow the incorporation of real sensors of a satellite such as gyros and star trackers in Hardware-In-The-Loop (HIL) simulation loops [9]. However, actuators such as reaction wheels or gas-jet thrusters have been simulated. The main idea in HIL simulation is that of incorporating a part of real hardware in the simulation loop during the system development [10]. Rather than testing the control algorithm on a purely mathematical model of the system, one can use real hardware in the simulation loop [10, 11]. This allows for detailed measurement for accurate performance assessment of the system under the test. The concept of the HIL methodology has also been utilized for design and implementation of various laboratory testbeds to study the dynamic coupling between a space-manipulator and its host spacecraft operating in free space [1, 12–14]. A system called the Vehicle Emulation System Model II (VES II) permits the experimental evaluation of planning and control algorithm for mobile terrestrial and space robot systems by using the so-called "admittance control" [13].

The existing impedance-controller based HIL simulators only compensate for the effect of gravity wrench on the force/moment measurement, while the effect of the payload's inertial forces (the test spacecraft in our case) has not been taken into account. Heavy payloads, however, not only changes the manipulator dynamics but also, incorporate significant inertial as well as gravitational force components into the measurement that can fail a conventional impedance controller to achieve the desired dynamics.

In this paper, we propose a method to control a manipulator with a heavy payload, e.g., a test spacecraft, so that the closed-loop system dynamics with respect to external force be as if the payload is with inertia properties corresponding to a flight spacecraft. Fig. 1 schematically illustrates a manipulator carrying a heavy payload, e.g., a scale model of the flight spacecraft. A six-axis force-moment sensor is installed at the interface of the payload and the manipulator, for sensing the external forces – for instance, firing thrusters – superimposed by gravitational and inertial forces. Upon measurement of the wrist force-moment and the joint angles and velocities, the signals are used by a control system that moves the manipulator and the test spacecraft with it appropriately. Such a setup allows virtually testing the actual control system, electronics, sensors, and actuators of a spacecraft in a closed-loop configuration in the laboratory environment. The distinct contribution of this work is a control system which incorporates dynamics models of the test spacecraft (payload), flight spacecraft as well as the manipulator to accurately replicate the motion dynamics of the flight spacecraft using a scaled mockup, as presented in Section 2.2. Notably, the controller can compensate for the inertial forces of the payload without needing any acceleration measurement; this is not

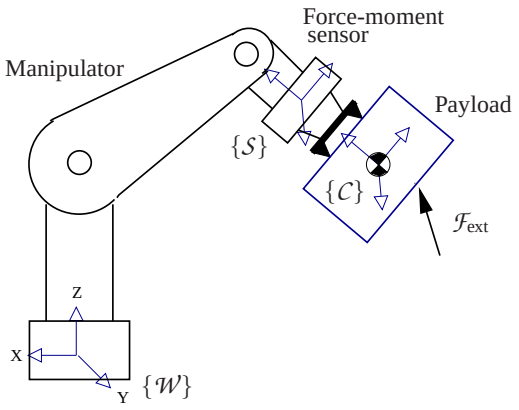

Figure 1. A manipulator carrying a heavy payload.

attainable with the conventional admittance controllers. A calibration procedure to precisely null out the static component of the F/M sensor in addition to sensitivity analysis are presented in Section 3. Section 4 is devoted to emulation of spacecraft having flexible appendages, e.g., solar panels. Finally, experimental results obtained from a robotic setup for spacecraft emulation with a milli-g accuracy are presented in Section 5.

2 Control System

2.1 Dynamics Model

The translational and the rotational motion dynamics of a *flight spacecraft* can be conveniently expressed in a body-fixed frame $\{C_s\}$ as

$$M_s\dot{\nu}_s + h_s(\nu_s) = \mathcal{F}_{\text{ext}}, \tag{1}$$

where

$$M_s = \text{diag}\{m_s I,\, I_{C_s}\}\,, \quad h_s(\nu_s) = \begin{bmatrix} m_s\omega_s \times v_s \\ \omega_s \times I_{C_s}\omega_s \end{bmatrix},$$

I denotes the identity matrix, m_s and I_{C_s} are the spacecraft mass and inertia tensor, $\nu_s^T = [v_s^T\ \omega_s^T]$ is the generalized velocity including the components of the linear velocity v_s and angular velocity ω_s of the spacecraft CM, and $\mathcal{F}_{\text{ext}}$ is the generalized external forces. It is worth mentioning that estimation of the other sources of external forces and torques such as gravity gradient, thin-air drag, and solar pressure can be added to the right-hand side (RHS) of (1) to achieve a more accurate result.

Fig. 1 illustrates the *test spacecraft* held by a manipulator. The test spacecraft is of mass and inertia m_m and I_{C_m}, respectively, that are different from those of the flight spacecraft. The F/M sensor installed in the mechanical interface of the manipulator and the test spacecraft allows us to measure the force/moment

interactions between the two systems. The coordinate-frame $\{W\}$ is fixed to the manipulator base and, the origin of body-fixed frame $\{C\}$ is chosen to be coincident with the CM of the test spacecraft, and its orientation with respect to frame $\{W\}$ is represented by the rotation matrix R. The test spacecraft is exposed to three different forces: the external force $\mathcal{F}_{\text{ext}}$, gravitational force $\mathcal{F}_g$, and force interaction between the test spacecraft and the manipulator $\mathcal{F}_s$ that is measured by the F/M sensor. Note that $\mathcal{F}_s$ is expressed in the body-fixed coordinate frame $\{S\}$ coincident with the sensor coordinate and parallel to $\{C\}$. Thus

$$\mathcal{F}_g = \begin{bmatrix} m_m g R^T k \\ 0 \end{bmatrix}, \tag{2}$$

where unit vector k is aligned with the gravity vector [1] which is expressed in the manipulator's base frame $\{W\}$, and $g = 9.81$ m/s^2. Similar to (1), the dynamics of the test spacecraft can be described by

$$\begin{aligned} M_m \dot{\nu} + h_m(\nu) &= -T\mathcal{F}_s + \mathcal{F}_g + \mathcal{F}_{\text{ext}} \\ &= -\mathcal{F}_{sg} + \mathcal{F}_{ext}. \end{aligned} \tag{3}$$

where T denotes the transformation from frame $\{S\}$ to $\{C\}$, i.e.

$$T = \begin{bmatrix} I & 0 \\ -[c\times] & I \end{bmatrix}, \quad [c\times] = \begin{bmatrix} 0 & -c_z & c_y \\ c_z & 0 & -c_x \\ -c_y & c_x & 0 \end{bmatrix},$$

vector c denotes the location of the center-of-mass and

$$\mathcal{F}_{sg} \triangleq T\mathcal{F}_s - \mathcal{F}_g. \tag{4}$$

2.2 Control Law

We assume that both the test and flight spacecraft experience the same actuation force $\mathcal{F}_{\text{ext}}$, and that their generalized velocities are the same, i.e., $\nu = \nu_s$. Under these assumptions, we can say the test spacecraft is dynamically equivalent to the flight spacecraft if they produce identical accelerations, i.e., $\dot{\nu} = \dot{\nu}_s$. However, the accelerations are governed by two different equations of motion, and hence, in general, $\dot{\nu} \neq \dot{\nu}_s$. Nevertheless, it is possible to achieve dynamical similarity if the manipulator is properly controlled. To this end, we define an estimation of the acceleration $\dot{\nu}^\star$ that is obtained by subtracting (3) from (1), i.e.,

$$M_\Delta \dot{\nu}^\star + h_\Delta = \mathcal{F}_{sg}, \tag{5a}$$

where

$$M_\Delta \triangleq \begin{bmatrix} (m_s - m_m)I & 0 \\ 0 & I_{C_s} - I_{C_m} \end{bmatrix}, \tag{5b}$$

$$h_\Delta \triangleq \begin{bmatrix} (m_s - m_m)\omega \times v \\ \omega \times (I_{C_s} - I_{C_m})\omega \end{bmatrix}. \tag{5c}$$

Assumption 1. *In the followings, we assume that M_Δ is a non-singular matrix, i.e.,*

$$m_s \neq m_m \quad \textit{and} \quad \lambda_i(I_{C_s} - I_{C_m}) \neq 0 \quad \forall i = 1, \cdots 3, \tag{6}$$

where $\lambda_i(\cdot)$ denotes the ith eigenvalue of matrix $(\cdot)$.

Notice that $\dot{\nu}^\star$ does not have any physical meaning, rather it is just a definition. Let $J = \begin{bmatrix} J_v^T & J_\omega^T \end{bmatrix}^T$ represent the manipulator Jacobian expressed in the coordinate frame $\{C\}$, where sub-matrices J_v and J_ω denote the translational and rotational Jacobians, respectively. That is $v(q,\dot{q}) = J_v\dot{q}$ and $\omega(q,\dot{q}) = J_\omega\dot{q}$, where q is the vector of joint angles. The time derivative of the velocity equation leads to

$$\dot{\nu} = J\ddot{q} + \dot{J}\dot{q}. \tag{7}$$

In view of equations (7) and (5a) and Assumption 1, we define $\ddot{q}^\star$ to be an estimation of the joint accelerations as

$$\ddot{q}^\star \triangleq J^{-1}(\dot{\nu}^\star - \dot{J}\dot{q}) \tag{8a}$$

$$= J^{-1}M_\Delta^{-1}\mathcal{F}_{sg} - J^{-1}\big(N + \dot{J}\big)\dot{q}, \tag{8b}$$

with $M_\Delta^{-1}h_\Delta = N\dot{q}$ and

$$N(q,\dot{q}) \triangleq \begin{bmatrix} [J_\omega\dot{q}\times]J_v \\ (I_{C_s} - I_{C_m})^{-1}[J_\omega\dot{q}\times](I_{C_s} - I_{C_m})J_\omega \end{bmatrix}.$$

Note that (8b) is obtained assuming that kinematic singularity does not occur.

Assume that the manipulator dynamics are characterized by inertia matrix $M_r(q)$ and the nonlinear vector $h_r(q,\dot{q})$, which contains Coriolis, centrifugal and gravitational terms. One can show that the equations of motion of the combined system of the manipulator and the payload can be written in the standard form as:

$$M_t\ddot{q} + h_t(q,\dot{q}) = \tau + J^T\mathcal{F}_{\text{ext}} \tag{9a}$$

[1] If the z-axis of the coordinate frame $\{W\}$ is perfectly parallel to the earth's gravity vector, then $k^T = [\,0\ 0\ -1\,]$.

where τ denotes the joint torques, and

$$M_t(q) \triangleq J^T M_m J + M_r(q), \tag{9b}$$

$$h_t(q,\dot{q}) \triangleq h_r(q,\dot{q}) + J^T h_m(\dot{q}) + J^T M_m \dot{J}\dot{q} - m_m g J_v^T R^T k. \tag{9c}$$

Now, the objective is to force the manipulator to follow the trajectory dictated by (8b). To achieve this goal, one can use the inverse-dynamics controller based on the complete model (9a), i.e.,

$$\tau = M_t(q)\ddot{q}^\star + h_t(q,\dot{q}) - J^T \mathcal{F}_{\text{ext}}^\star + M_t(q)\Big(K_d\big(\int \ddot{q}^\star dt - \dot{q}\big) + K_p\big(\int\int \ddot{q}^\star dt - q\big)\Big), \tag{10}$$

with $K_d = k_d I$ and $K_p = k_p I$ being the controller gains and $\mathcal{F}^\star$ being an estimation of the external force. In the following analysis, we will show that the above inverse-dynamics controller in conjunction with a force estimator lead to exponential stability. Let $\tilde{\ddot{q}} \triangleq \ddot{q}^\star - \ddot{q}$ denotes the joint acceleration error, then the corresponding Cartesian acceleration error is readily obtained from definition (8a) as

$$\dot{\tilde{\nu}} \triangleq \dot{\nu}^\star - \dot{\nu} = J(q)\tilde{\ddot{q}}. \tag{11}$$

Substitution of $\dot{\nu}^\star$ obtained from (5a) into the above equation yields

$$\dot{\nu} = M_\Delta^{-1}\mathcal{F}_{sg} - N\dot{q} - J\ddot{\tilde{q}}.$$

Now, upon substitution of the acceleration from the above into (3), we can write the expression of the external force as:

$$\mathcal{F}_{ext} = \mathcal{F}_{\text{ext}}^\star + \tilde{\mathcal{F}}_{\text{ext}},$$

where

$$\mathcal{F}_{\text{ext}}^\star = \big(I + M_m M_\Delta^{-1}\big)\mathcal{F}_{sg} + h_m - M_m N\dot{q} \tag{12}$$

is the estimation of the external force and

$$\tilde{\mathcal{F}}_{ext} = -M_m J\ddot{\tilde{q}} \tag{13}$$

is the force estimation error. Clearly, the force estimation error goes to zero only if the acceleration error does so. We will show that under a mid condition, controller (10) in conjunction with force estimator (12) results in exponential stabling of the motion and force errors. To this end, substitution of $\mathcal{F}_{\text{ext}}^\star$ and $\ddot{q}^\star$ obtained from (12) and (8b), respectively, into (10) yields the expression of the control law as:

$$\tau = J^T\big(M_{Cr}(q)M_\Delta^{-1} - I\big)\mathcal{F}_{sg} + h_r(q,\dot{q}) - M_r(q)J^{-1}(N(q,\dot{q}) + \dot{J})\dot{q} - m_m g J_v^T R^T k + M_t(q)\Big(K_d\big(\int \ddot{q}^\star\,\mathrm{d}t - \dot{q}\big) + K_p\big(\int\int \ddot{q}^\star\,\mathrm{d}t - q\big)\Big), \tag{14}$$

where $M_{Cr} \triangleq J^{-T} M_r J^{-1}$ is the *Cartesian inertia* of the manipulator. Stability of closed-loop system remains to be proved. Knowing that (14) becomes equivalent to (12) if the force term, $\mathcal{F}_{\text{ext}}$, of the former equation is replaced by $\mathcal{F}_{\text{ext}}^\star = \mathcal{F}_{\text{ext}} - \tilde{\mathcal{F}}_{\text{ext}}$, we can arrive at the equations of the motion and force errors by substituting (14) into system (9a), i.e.,

$$M_t\big(\tilde{\ddot{q}} + K_d\dot{\tilde{q}} + K_p\tilde{q}\big) = -J^T\tilde{\mathcal{F}}_{\text{ext}}.$$

Moreover, we know that the force and acceleration errors are related by (13). Thus

$$M_r\tilde{\ddot{q}} + M_t\big(K_d\dot{\tilde{q}} + K_p\tilde{q}\big) = 0,$$

which can be rewritten as:

$$\tilde{\ddot{q}} + K_d\dot{\tilde{q}} + K_p\tilde{q} + Q(q)\big(K_d\dot{\tilde{q}} + K_p\tilde{q}\big) = 0, \tag{15}$$

where

$$Q \triangleq M_r^{-1}\big(JM_mJ^T\big). \tag{16}$$

We will show that system (15) remains stable if the coefficient matrix of the additive term, Q, is sufficiently small. Let assume that $x^T = [\tilde{q}^T \quad \dot{\tilde{q}}^T]$ represent the state vector. Then, (15) can be written as

$$\dot{x} = Ax + \varepsilon(t,x) \tag{17}$$

where

$$A = \begin{bmatrix} 0 & I \\ -K_p & -K_d \end{bmatrix} \quad \text{and} \quad \varepsilon(t,x) = -Q\begin{bmatrix} 0 \\ K_p\tilde{q} + K_d\dot{\tilde{q}} \end{bmatrix}.$$

Since the perturbation term ε satisfies the linear growth bound

$$\|\varepsilon\| \le \sqrt{k_p^2 + k_d^2}\|Q\|\|x\|,$$

system (17) is in the form of *vanishing perturbation* [15]. Moreover, since A is Hurwitz, there exists Lyapunov function

$$V(x) = x^T P x \tag{18}$$

with $P > 0$ satisfying

$$PA + A^T P = -I. \tag{19}$$

The derivative of $V(x)$ along trajectories of perturbed system (17) satisfies

$$\dot{V} \leq \left(-1 + 2\sqrt{k_p^2 + k_d^2}\lambda_{\max}(P)\|Q\|\right)\|x\|^2 \tag{20}$$

On the other hand, the solution of the Lyapunov equation (19) is given by

$$P = \frac{1}{2k_p k_d}\begin{bmatrix} k_p(k_p+1)+k_d^2 & k_d \\ k_d & k_p+1 \end{bmatrix},$$

which verifies

$$\lambda_{\max}(P) \leq \frac{(k_p+1)^2 + k_d^2}{2k_p k_d}.$$

Therefore, according to the stability theorem of perturbed system [15, p. 206], the origin of (17) is globally exponentially stable if

$$\|Q\| \leq \alpha(k_p, k_d) = \frac{k_p k_d}{\left((k_p+1)^2 + k_d^2\right)^{\frac{3}{2}}}. \tag{21}$$

Using the norm properties in (16), we obtain a conservative condition for the stability as:

$$\lambda_{\max}(M_m) \leq \alpha(k_p, k_d)\frac{\lambda_{\min}(M_r)}{\lambda_{\max}(JJ^T)}. \tag{22}$$

Now, if (21) is satisfied, then there must exist scalar $\Omega > 0$ such that $\|x\| \leq \|x(0)\|e^{-\Omega t}$. Therefore, it can be inferred from (15) that

$$\|\ddot{\tilde{q}}\| \leq ae^{-\Omega t}, \tag{23}$$

where $a = (k_p^2 + k_d^2)(1 + \|Q\|)\|x(0)\|$.

Now, we are ready to derive the input/output relation of the closed loop system under the proposed control law. Adding both sides of (3) and (5a) yields

$$M_s\dot{\nu} + M_\Delta\dot{\nu}^\star + h_s = \mathcal{F}_{\text{ext}}. \tag{24}$$

Finally, using (11) in (24), the equations of motion of the test spacecraft become

$$M_s\dot{\nu} + h_s(\nu) = \mathcal{F}_{\text{ext}} + \delta, \tag{25a}$$

where

$$\delta(t) = M_\Delta J\ddot{\tilde{q}} \tag{25b}$$

is a non-vanishing perturbation. Since J is always a bounded matrix, we can say

$$\sigma = \max_q \sqrt{\lambda_{\max}(J^T J)},$$

where $\lambda_{\max}(\cdot)$ denotes the maximum eigenvalue of a matrix. It follows from (23) and (25b) that

$$\|\delta\| \leq \sigma a\lambda_{\max}(M_\Delta)e^{-\Omega t}, \tag{26}$$

which means that the perturbation exponentially relaxes to zero from its initial value. The above development can be summarized in the following.

Proposition 1. *Let a rigid-body object with generalized inertia M_m attached to a manipulator with inertia M_r. Assume that the force/moment developed at the interface of the object and the manipulator is sensed and fed back to the manipulator according to the control law* (14)*. Moreover, assume that* (6) *and* (21) *are satisfied. Then, the motion of the object in response to external force $\mathcal{F}_{\text{ext}}$ obeys equation of motion of another rigid-body object characterized by generalized inertia M_s.*

2.3 Force Feedback Gain

Ideally, the controller of the emulating system can change the inertia of the test spacecraft to any desired value. However, there are constraints (6) and (22) on the inertia matrices of the test and flight spacecraft as well as the manipulator that must be considered in the design. Assuming a steady-state mode in which the control error reaches zero, we can express the torque-control input by

$$\tau = J^T(M_{Cr}M_\Delta^{-1} - I)\mathcal{F}_{sg} + \eta(q, \dot{q}), \tag{27}$$

where $\eta(q,\dot{q})$ represents the motion dependent portion of the feedback, while the first term in the RHS of equation (27) is force feedback. In the following we examine two extreme cases of the force feedback gain.

2.3.1 Zero Gain Equation (27) implies that the force feedback is disabled if $M_{Cr} = M_\Delta$ or

$$M_{Cr}(q) + M_m = M_s. \tag{28}$$

Clearly, to implement the emulation controller without force feedback requires satisfying (28) for all possible postures. However, with the exception of Cartesian manipulators, most manipulators are of configuration-dependent inertia matrix, whereas the spacecraft inertia are constant matrices. This means that the condition (28) can be satisfied only for few isolated postures at best. It is worth mentioning that the case of $M_s = M_m$ becomes a favorable condition if $M_{C_r} \equiv 0$, i.e., the manipulator inertia is negligible; see (28). However, a manipulator with zero mass (and zero joint friction) can be though of as an air-bearing simulator system, which has its own shortcomings as descried in Section 1.

2.3.2 Infinite Gain It is apparent from (27) that for the control torque effort to be bounded requires that M_Δ be a non-singular matrix, i.e., condition (6) is satisfied. At first glance, this result seems counterintuitive. But, it can be seen from (5a) that the acceleration and thus the subsequent motion trajectory can be uniquely estimated only if M_Δ is a full-rank matrix. It is also apparent from (1) and (3) that the only possibility for the flight and test spacecraft with the same mass and inertia to produce similar velocity and acceleration trajectories with respect to external force $\mathcal{F}_{ext}$ is that the interaction force $\mathcal{F}_{sg}$ becomes zero. Clearly, in such as case, it is not possible to predict the position and velocity trajectories from the estimated acceleration and hence the feedback is meaningless.

3 Simulating a Micro-G Environment

3.1 Precise Gravity Compensation

Performing a high-fidelity zero-g emulation critically relies on a precise force/moment feedback which, in turn, is determined by: (i) Accuracy of the gravity compensation; (ii) the resolution of the F/M sensor. These issues are discussed below.

3.1.1 Calibration The static components of the F/M sensor output include the sensor offset and the payload gravitational force, which are not distinguishable from each other. Nevertheless, if a sequence of sensor readings is recorded by locating the manipulator in several known poses, it is possible to identify the sensor offset together with all the gravity parameters that are required to null out the static components of the sensor.

If the gravity were completely compensated, then for every position we would have $\mathcal{F}_{sg} = 0$, i.e., $T(\mathcal{F}_s - \mathcal{F}_0) - \mathcal{F}_g = 0$, where $\mathcal{F}_0^T = \begin{bmatrix} f_0^T & n_0^T \end{bmatrix}$ denotes the sensor offset. Now, we consider $\{\mathcal{F}_0, m_m, c, k\}$ as the set of uncertain parameters that are be identified. Defining vector $w \triangleq m_m k$ and knowing that $[c\times]R^T w = -[(R^T w)\times]c$, we can break up $\mathcal{F}_s = T^{-1}\mathcal{F}_g + \mathcal{F}_0$ into two *linear regression* equations as

$$f_s = \begin{bmatrix} I & gR^T \end{bmatrix} \begin{bmatrix} f_0 \\ w \end{bmatrix}, \tag{29a}$$

$$n_s = \begin{bmatrix} I & -gm_m[(R^T k)\times] \end{bmatrix} \begin{bmatrix} n_0 \\ c \end{bmatrix}, \tag{29b}$$

where $\mathcal{F}_s^T = \begin{bmatrix} f_s^T & n_s^T \end{bmatrix}$. Now stacking p measurements $y_1^T = [f_{s1}^T, f_{s2}^T, \cdots, f_{sp}^T]$ and $y_2^T = [n_{s1}^T, n_{s2}^T, \cdots, n_{sp}^T]$, that are obtained by configuring the manipulator at p different positions $\{q_1, q_2, \cdots, q_p\}$, we can derive two linear matrix relation $y_1 = \Psi_1(q)\Theta_1$ and $y_2 = \Psi_2(q,\Theta_1)\Theta_2$ from (29a-29b), where vectors Θ_1 and Θ_2 contain the parameters of interest. Finally, assuming a sufficient number of independent equations, one can obtain the vectors of estimated parameters $\hat{\Theta}_1$ and $\hat{\Theta}_1$ consecutively by using the least squares method from

$$\hat{\Theta}_1 = \Psi_1^+ y_1, \quad \text{and} \quad \hat{\Theta}_2 = \Psi_2^+(\hat{\Theta}_1) y_2,$$

where $\Psi_i^+ = \Psi_i^T(\Psi_i \Psi_i^T)^{-1}$ is the pseudo-inverse of Ψ_i. Note that the mass and the gravitational vector can be retrieved from

$$\hat{m}_m = \|\hat{w}\| \quad \text{and} \quad \hat{k} = \frac{\hat{w}}{\|\hat{w}\|}.$$

3.1.2 Position Errors and Accuracy of the Gravity Compensation Error between the measured joint angles used by the gravity compensator and the true joint angles will result in a small residual static force acting on the payload. One source of this error is measured quantization. In order to minimize the residual force induced by the quantization as much as possible, we need to employ high-resolution encoders at the joints so that the induced error becomes at least comparable to the F/M sensor resolution. In the following we relate the errors in the gravity compensation and the that of joint angles.

Assume that Δq and Δf_s denote small errors in measured joint angles and the computed gravity force, respectively. Using the Taylor series of (29a) leads to

$$\|\Delta f_s\| \le g m_m \left\| \frac{\partial}{\partial q} R^T(q) k \right\| \|\Delta q\|. \tag{30}$$

Using the facts that all elements of the rotation matrix are sinusoidal functions of q and that k is a unit vector, one can show that a conservative bound on the first norm of the RHS of (30) is 6. Thus, a bound on the force error can be found as

$$\|\Delta f_s\| \leq 6 g m_m \|\Delta q_\cdot\| \tag{31}$$

Similar argument shows that a conservative bound on the magnitude of moment error Δn_s can be found as

$$\|\Delta n_s\| \leq 6 g m_m \|c\| \|\Delta q_\cdot\| \tag{32}$$

3.2 Assessing the Quality of the Micro-Gravity Environment

Emulation in a zero-gravity environment requires the static component of the F/M sensor is perfectly nulled out. However, in practice, this requirement can not be completely satisfied due to errors. A natural question rises; what is the quality of the emulator in simulating a weightlessness environment? To answer this question, let us assume that $\delta \bar{f}_{sg}$ denote the average magnitude error of the compensated F/M sensor output over several payload static poses. Then, the average acceleration introduced to the emulating system can be simply obtained by dividing the magnitude of this force by the inertia of the spacecraft being simulated. Normalizing the acceleration w.r.t. the Earth gravity constant, we define the following dimensionless index

$$\gamma \triangleq \frac{\delta \bar{f}_{sg}}{g m_s} \times 10^6 = \frac{\| \sum_i^n f_{s_i} - \Psi_{1_i} \hat{\Theta}_1 \|}{n g m_s} \times 10^6 \tag{33}$$

to measure the virtual gravity of the simulated environment. In other words, the payload (test spacecraft) experiences as though it moves under a gravitational field with intensity of $\gamma \cdot g$ rather than a zero-g environment. It is worth pointing out that γ can be also interpreted as the drift exhibited by the emulation system. Similarly, the micro-gravity environment for the rotational motion can be defined as

$$\frac{\| \sum_i^n n_{s_i} - \Psi_{2_i} \hat{\Theta}_2 \|}{n g \|c\| m_m} \times 10^6.$$

3.2.1 Resolution of F/M Sensor

At best, the force error $\delta \bar{f}_{sg}$ can be reduced down to the resolution of the F/M sensor. The resolution of a F/M sensor depends on its sensing range; a sensor with large sensing range tends to have lower resolution and vice versa. Since the F/M sensor is located at the manipulator-payload interface, the sensor should be selected so that its sensing range matches the weight of payload, i.e., the test spacecraft. Therefore, the ratio of the sensor resolution to its sensing range is the emulation system limitation in achieving the lowest micro-g.

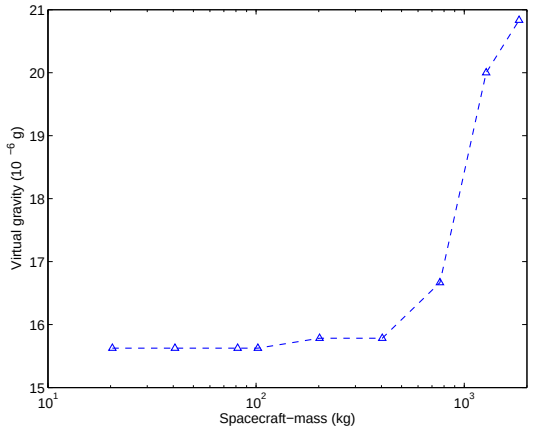

Figure 2. The best achievable micro-g environment, computed from the resolutions of a series of commercial F/M sensors, for emulation of spacecraft with different masses.

Fig. 2 illustrates the best achievable micro-g's versus different spacecraft masses that is calculated from the resolutions and the sensing ranges of the commercial ATI F/M sensors [16]. Here, we assume that the scaling factor of the emulated spacecraft is two. It is evident from the figure that in the emulation of small to medium size spacecraft with mass of up to 500kg, the sensor resolution is sufficient for achieving accuracy of $16 \times 10^{-6} g$ (it almost remains constant in that range). However, the value of the virtual gravity dramatically increases, when the spacecraft mass exceeds that critical mass. This is due to the fact that commercial F/M sensors with large load capacity come with relatively low resolution. In order to improve the γ factor, one may use a mechanism to counter the effects of gravity in rigid-bodies [17–20]. For example, using a passive counterweight [17] can substantially reduce the static load on the F/M sensor, thereby allowing smaller and more precise sensor to be selected. The main disadvantage of this method is introduction of additional inertia. However, this is not an issue here because the controller can scale the inertia of the payload down or up to any desired value.

4 Emulation of Flexible Spacecraft

Many spacecraft have flexible appendages, e.g. satellites with solar panels, that can significantly affect their dynamics. However, testing a flexible spacecraft in a 1-g environment poses many difficulties due to large deformation induced by gravity. Indeed, the structure of a solar panel cannot even hold itself against gravity when it is fully deployed. Moreover, the location of the

CM of a flexible spacecraft is no longer fixed as it depends on the flexural coordinates whose direct measurement is not usually available. In the following, we extend the emulation concept for the case where the test spacecraft is rigid while the target flight spacecraft is flexible. It is assumed that the actuators are mounted to the rigid part of the test spacecraft. The test spacecraft lacks any flexible hardware, such as solar panels. Yet, motion perturbation caused by the flexible appendages is generated by simulation and then superimposed on the trajectories that subsequently drive the manipulator.

Let ξ denote the flexural coordinates of a flexible spacecraft. Then, the equations of motion for the entire system can be written in the partitioned mass matrix form

$$\begin{bmatrix} M_s & M_{sf} \\ M_{sf}^T & M_f \end{bmatrix} \begin{bmatrix} \dot{\nu} \\ \ddot{\xi} \end{bmatrix} + \begin{bmatrix} h_{sr}(\nu, \xi, \dot{\xi}) \\ h_{sf}(\nu, \xi, \dot{\xi}) \end{bmatrix} = \begin{bmatrix} \mathcal{F}_{\text{ext}} \\ 0 \end{bmatrix}, \tag{34}$$

where M_f is the flexural inertia matrix, M_{sf} is the cross inertia matrix, h_{sr} and h_{sf} are the nonlinear vectors associated with the rigid and flexural coordinates. Analogous to the case of rigid spacecraft, subtracting equation (34) from (3) eliminates $\mathcal{F}_{\text{ext}}$ from the the equations of motion. Defining $\bar{M}_\Delta = M_\Delta - M_{sf} M_f^{-1} M_{sf}^T$ and $h_\Delta = h_{sr} - h_m$, we can write the accelerations of the rigid and the flexural coordinates by

$$\ddot{q}^\star = -J^{-1}(N + \dot{J})\dot{q} - J^{-1}\bar{M}_\Delta^{-1} M_{sf} M_f^{-1} h_{sf} + \bar{M}_\Delta^{-1} \mathcal{F}_{sg}, \tag{35}$$

and

$$\ddot{\xi} = -M_f^{-1}(I + M_f^{-1} M_{sf}^T M_{sf} M_f^{-1}) h_{sf} - M_f^{-1} M_{sf}^T \bar{M}_\Delta^{-1}(\mathcal{F}_{sg} - h_\Delta). \tag{36}$$

Equation (35) can be substituted in (14) to obtain the control law. However, to calculate the acceleration from (35) requires the value of the flexural states because h_{sr} and h_{sf} are functions of ξ and $\dot{\xi}$. An estimation of the flexural states can be obtained by simulation. First, the acceleration of the flexural coordinate can be computed by making use of the acceleration model (36), and then the flexural states are obtained as a result of numerical integration.

5 Experiment

5.1 Setup Description

This section describes the implementation of the proposed spacecraft simulator using a Titan II Schilling industrial manipulator at the robotics laboratory of the Canadian Space Agency (CSA), see Fig. 3. A mockup of a satellite, which weights 11 kg, is mounted on the wrist of the manipulator. The objective is to control the manipulator so that the motion of the mockup satellite resulting from external forces matches that of a free-floating object in zero-g environment.

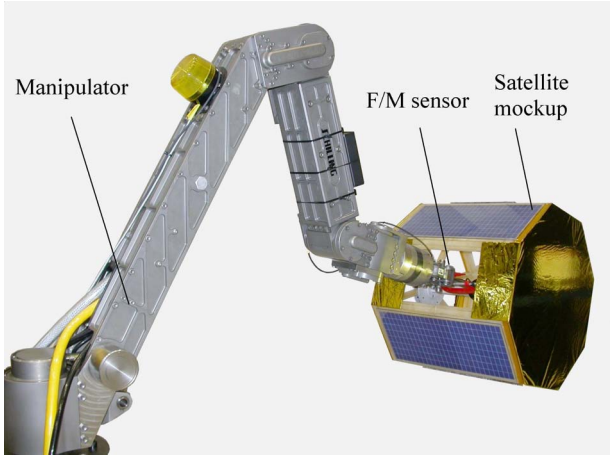

Figure 3. The hydraulic manipulator for the spacecraft simulator.

The force/moment interaction between the manipulator and the satellite mockup were measured by a six-axis ATI force-moment sensor (Gamma type). With the resolution 0.05 N in force and 0.003 Nm in moment. The sensing ranges of the sensor are 130 N and 5 Nm. The robot joint angles were measured by 16-bit encoders. Therefore, the maximum induced error in the gravity compensation is about 0.06 N (according to (31)), that is comparable to the resolution of the force sensor. Also, every hydraulic actuator is equipped with two pressure transducers that measure the pressure of its chambers. Also, each joint has its own torque controller that forces its hydraulic actuator to generate the desired torque requested by the control system. A detailed description of the joint-torque controller is given in [21].

The controller was developed using Simulink and matrix manipulation was performed by using the DSP Blockset of Matlab/Simulink [22]. The Real-Time Workshop package [23] generated portable C code from the Simulink model which was executed on a QNX real-time operating system.

5.2 Micro-Gravity Environment

As mentioned in Section 3.2, the effect of gravity may not be completely compensated for due to errors. Fig. 4 illustrates the Euclidean norms of the difference between the F/M sensor outputs and the estimated values when the manipulator is configured at several poses in a quasi-static manner. Therefore, given the force error, we compute the virtual gravity of the emulation system from (33) to be as

$$1.1 \times 10^{-3} g.$$

This shows the particular setup can emulate a milli-g environment rather than a micro-g environment.

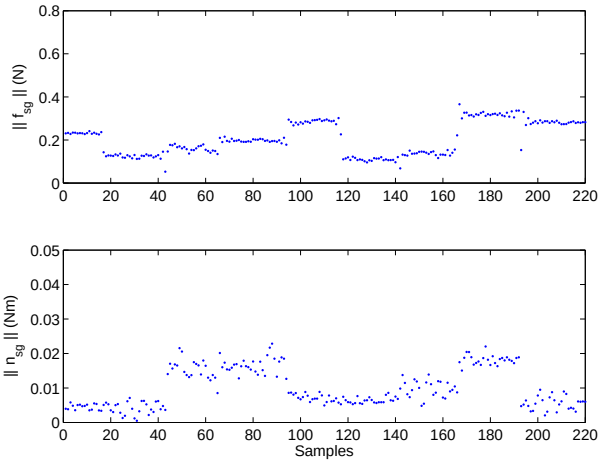

Figure 4. The Euclidean norms of the difference between the F/M sensor outputs and the estimated values.

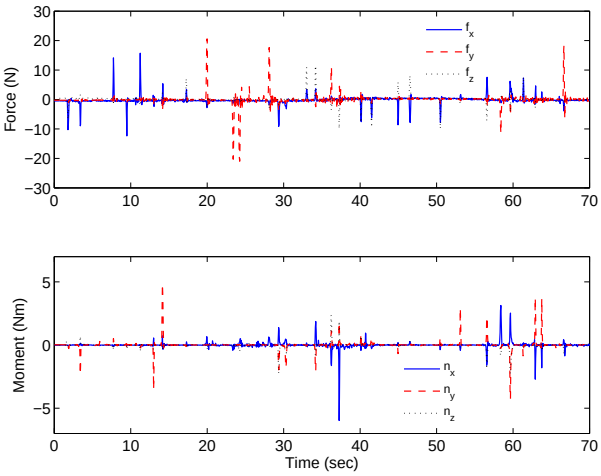

Figure 5. The force and moment after gravity compensation.

5.3 Dynamic Response Test

Fig. 5 shows trajectories of the forces and moments (after gravity compensation) due to external force impulses applied by hand. The subsequent trajectories of the linear and angular velocities of the mockup satellite are illustrated in Fig. 6 (top). The simulated velocity profiles according to the force/moment inputs are also depicted in Fig. 6 (bottom), that reassemble the velocity profiles obtained from HIL simulation. Note that, in the simulation, the baseline noises in the force and moment signal, which persist between impulses, are removed by a dead-zone filter. In other words, only responses to the force and moment impulses are simulated.

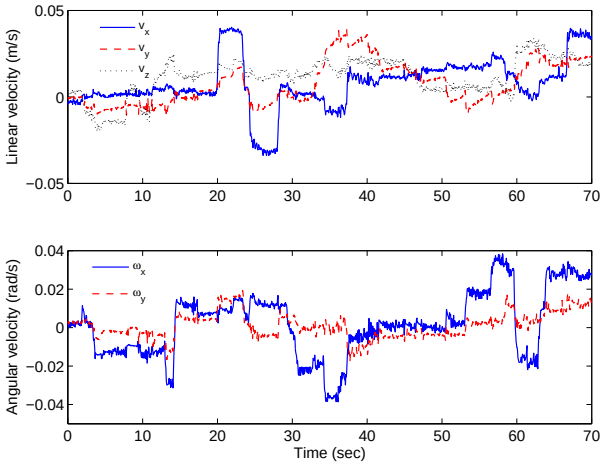

(a)

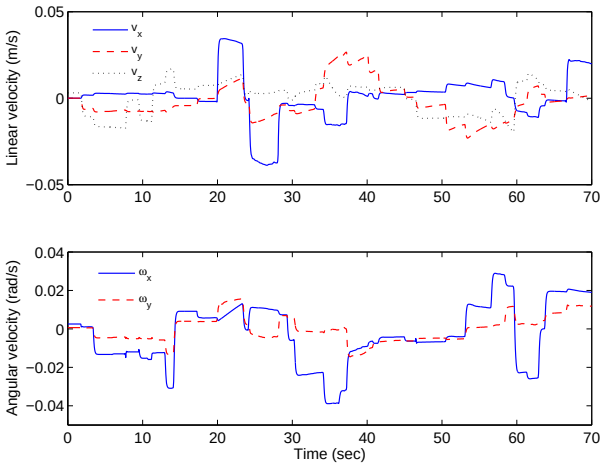

(b)

Figure 6. Trajectories of the linear and angular velocities of the mockup satellite obtained from the HIL simulation (a) versus those of the simulation (b).

6 Conclusions and Discussions

A control system for a manipulator carrying a rigid-body payload has been developed in order to modify the motion dynamics of the combined system in consequence of external according to that of a free-floating body which has different inertial properties from the payload. This allowed zero-g emulation of the scaled prototype of a spacecraft (with non-negligible inertia) in a 1-g laboratory environment. It was shown that the controller in conjunction with the motion and force estimators could drive the manipulator so as to achieve dynamical similarity between the test and flight spacecraft. Notably, the controller can compensate for the inertial forces of the heavy payload (test spacecraft) without needing any acceleration measurement.

The stability of the closed loop system was analytically in-

vestigated. The results showed that system remains stable provided that mass and inertia of the test and flight spacecraft are not the same and that the norm of the inertia ratio of the payload to manipulator is upper bounded by a scaler which is a function of the controller gains. Finally, the methodology was extended for emulation of spacecraft having flexible appendages, e.g. solar panels.

A calibration procedure to precisely null out the static component of the F/M sensor was developed that tunes the gravity, kinematic, and sensor parameters all together. A sensitivity analysis showed that the position and force sensors have to be with specified resolutions in order to achieve a certain level of microgravity. Finally, the emulation system was underpinned by experimental results obtained from a robotic setup for emulation of a satellite mockup.

REFERENCES

[1] Yoshida, K., 1995. "Experimental study on the dynamics and control of a space robot with the experimental free-floating robot satellite (EFFORTS) simulator". *Advanced Robotics*, **9**(6), pp. 583–602.

[2] Yoshida, K., 2003. "Engineering test satellite VII flight experiment for space robot dynamics and control: Theories on laboratory test beds ten years ago, now in orbit". *The Int. Journal of Robortics Research*, **22**(5), pp. 321–335.

[3] Schwartz, J. L., Peck, M. A., and Hall, C. D., 2003. "Historical review of air-bearing spacecraft simulators". *AIAA Journal of Guidance, Control, and Dynamics*, **26**(4), pp. 513–522.

[4] Choset, H., and Kortenkamp, D., 1999. "Path planning and control for free-flying inspection robot in space". *Journal of Aerospace Engineering*, **12**(2), pp. 74–81.

[5] Schubert, H., and How, J., 1997. "Space constrauction: An experimental testbed to develop enabling technologies IEEE". In Proccedingsof the Confernce on Telemanipulator and Telepresence Technologies IV, pp. 179–188.

[6] Matunaga, S., Yoshihara, K., Takahashi, T., Tsurumi, S., and Ui, K., 2000. "Ground experiment systems for dual-manipulator-based capture of damaged satallites". In IEEE Int. Conference on Intelligent Robots and Systems, pp. 1847–1852.

[7] Kawamoto, S., Matsumoto, K., and Wakabayashi, S., 2001. "Ground experiment of mechanical impulse method for uncontrollable satellite capturing". In Procceding of the 6th Int. Symposium on Artificial Intelligence and Robotics & Automation in Space: I-SAIRAS.

[8] Peck, M. A., Miller, L., Cavender, A. R., Gonzalez, M., and Hintz, T., 2003. "An airbearing-based testbed for mmentum-control systems and spacecraft line of sight". *American Astronautical Society, ASS*, February, pp. 3–127.

[9] Ng, A. C., and Golla, D. F., 1999. "Odin attitude control systems testing - an international collaboration". In 4th ESA International Conf. On Spacecraft Guidance, Navigation and Control Systems.

[10] Bacic, M., 2005. "On hardware-in-the-loop simulation". In IEEE Confernece on Decision and Control, pp. 3194–3198.

[11] Aghili, F., Namvar, M., and Vukovich, G., 2006. "Satellite simulator with a hydraulic manipulator". In IEEE Int. Conference on Robotics & Automation, pp. 3886–3892.

[12] Sato, Y., Ejiri, A., Iida, Y., Kanda, S., Maruyama, T., Uchiyama, T., and Fujii, H., 1991. "Mico-g emulation system using constant-tension suspenstion for a space manipulator". In IEEE Int. Conference on Robotics and Automation, pp. 1893–1900.

[13] Dubowsky, S., Durfee, W., Kulinski, A., Müller, U., Paul, I., and Pennington, J., 1994. "The design and implementation of a laboratory test bed for space robotics: The ves mod II". In ASME Conf. DE-Vol. 72, Robotics: Kinematics, Dynamics and Control, pp. 99–108.

[14] Akima, T., Tarao, S., and Uchiyama, M., 1999. "Hybrid micro-gravity simulator consisting of a high-speed parallelrobot". In IEEE Int. Conference on Robotics and Automation, pp. 901–906.

[15] Khalil, H. K., 1992. *Nonlinear Systems*. Macmillan Publishing Company, New-York.

[16] ATI INDUSTRIAL AUTOMATION, 2007. *Multi-Axis Force/Torque Sensor, 2007 Catalog*.

[17] White, G. C., and Yangsheng, X., 1994. "An active vertical-direction gravity compensation system". *IEEE Trans. on Instrumentation & Measurement*, **43**(6), pp. 786–792.

[18] Rahman, T., Ramanathan, R., Seliktar, R., and Harwin, W., 1995. "A simple technique to passively gravity-balance articulated mechanisms". *ASME Jouirnal of Mechanical Design*, **117**(4), pp. 655–658.

[19] Gopalswamy, A., Gupta, P., and Vidyasagar, M., 1992. "A new parallelogram linkage configuration for gravity compensationusing torsional springs". In IEEE Int. Conference on Robotics & Automation, pp. 664–669.

[20] Ulrich, N., and Kumar, V., 1991. "Passive mechanical gravity compensation for robot manipulators". In IEEE Int. Conference on Robotics & Automation, pp. 1536–1541.

[21] Namvar, M., and Aghili, F., 2003. "A combined scheme for identification and robust toque control of hydraulic actuators". *ASME Journal of Dynamic Systems, Measurement, and Control*, **125**, December, pp. 595–606.

[22] THE MATHWORKS INC., 1998. *DSP Blockset for Use with Simulink, User's Guide*. 24 Prime Parlway, Natick, MA 011760-1500.

[23] THE MATHWORKS INC., 2002. *Real-Time Workshop for Use with Simulink*, 5th ed. 3 Apple Hill Drive, Natick, MA 011760-2098.